ISSN 1064-2269, Journal of Communications Technology and Electronics, 2023, Vol. 68, No. 9, pp. 983–988. © Pleiades Publishing, Inc., 2023.
Russian Text © The Author(s), 2023, published in Radiotekhnika i Elektronika, 2023, Vol. 68, No. 9, pp. 897–903.

ON THE 70th ANNIVERSARY OF THE INSTITUTE OF RADIOENGINEERING AND ELECTRONICS, RUSSIAN ACADEMY OF SCIENCES

Comparison of Methods for Calculation of Superconducting Integrated Structures Using Semi-Analytical Calculation and 3D Numerical Simulation

F. V. Khan[a, b, *], A. A. Atepalikhin[a, b], L. V. Filippenko[a], and V. P. Koshelets[a]

[a] *Kotelnikov Institute of Radioengineering and Electronics, Russian Academy of Sciences, Moscow, 125009 Russia*
[b] *Moscow Institute of Physics and Technology, Dolgoprudnyi, Moscow oblast, 141701 Russia*
**e-mail: khanfv@hitech.cplire.ru*

Received May 10, 2023; revised May 10, 2023; accepted May 25, 2023

Abstract—Superconducting integrated structures are simulated in a frequency range of 300–750 GHz using two methods: (i) ABCD matrices related to each element of the circuit and (ii) Ansys HFSS software. The surface impedance of superconducting films is numerically calculated using expressions from the Mattis–Bardeen theory. For samples with microstrip line widths of less than one quarter of the wavelength, both models are in qualitative agreement with each other and with experimental data. It is shown that an increase in the width of the lines and the geometric dimensions of other circuit elements leads to generation of transverse modes and non-plane wave front of waves propagating along the lines, which causes discrepancy between the semi-analytical and numerical calculations, while the latter are in agreement with the experiment for all samples.

DOI: 10.1134/S1064226923090115

INTRODUCTION

Devices of modern superconducting electronics are widely used in both applied areas and fundamental research due to unique characteristics that are impossible for devices based on alternative principles: the noise temperature of superconducting receivers reaches several values of the quantum limit [1–3] and nonlinearity near the gap voltage at sufficiently low temperatures is the strongest known to date [4]. Mixers based on Josephson tunnel junctions are the main components in receiving systems of ground-based submillimeter telescopes (e.g., ALMA telescope (https://almaobservatory.org), APEX telescope (https://www.apex-telescope.org), and complex under construction on the Suffa plateau (http://asc-lebedev.ru/index.php?dep=16)). The use of superconducting mixers is also planned in upcoming space missions (for example, Millimetron (https://millimetron.ru/). A superconducting heterodyne receiver was used in the study of human body radiation in the terahertz (THz) range [5]. Similar devices were also used to analyze the composition of the atmosphere both in laboratory [6] and on board a high-altitude balloon [7].

In almost all cited works, superconducting devices have been fabricated as planar integrated structures that combine microstrip lines, antennas, and distributed and lumped Josephson junctions. The efficiency of superconducting receivers depends on both parameters of single Josephson junctions and matching of circuit elements [7, 8]. In this regard, it is expedient to consider design of devices with the necessary parameters.

On the one hand, such devices can be designed using the ABCD matrix method, which is widely used in calculation of electrical circuits [9, 10] and, on the other hand, we can directly calculate the field distribution in the structure using commercial 3D simulators, for example, Ansys HFSS (https://www.ansys.com/products/electronics/ansys-hfss). This work compares the results of both methods with each other and with experimental data.

1. SIMULATED DEVICES

Figure 1 schematically shows a device under study. Such integrated circuits are used to study various superconducting detectors and generators in the THz range [11, 12] and also serve as components of a superconducting integrated heterodyne receiver [2, 13].

A flux-flow oscillator (FFO) based on long Josephson junction is used as a generator of microwave signal (see Fig. 1). The power emitted by the FFO propagates along the matching network *2, 3* and *4* (see Fig. 1) and is detected using a lumped superconductor–insulator–superconductor (SIS) Josephson junction (position is indicated with arrow). Figure 2 presents the current-voltage characteristic (IVC) of the SIS junc-

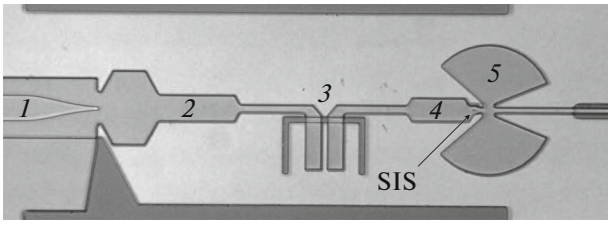

Fig. 1. Microphotograph of the circuit of the superconducting microwave structure under study: (*1*) microwave signal generator on FFO, (*2*) step impedance transformer between FFO and (*3*) dc block, (*4*) step impedance transformer between SIS detector and dc block, and (*5*) radial stub for detuning of the capacitance of the SIS junction.

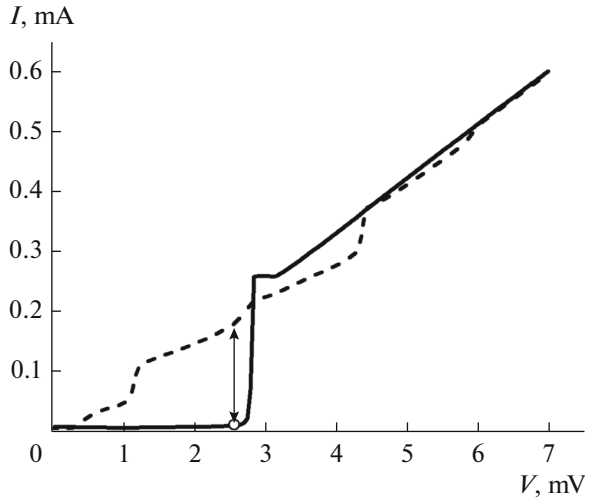

Fig. 2. Experimental IVCs of the SIS junction (dashed line) in the presence of external alternating electromagnetic field with a frequency of 400 GHz and (solid line) in the absence of the field. The pump current at the working point (shown with arrow) is used to determine the incoming power. The critical current is suppressed using magnetic field.

tion with the critical current suppressed by magnetic field. The presence of an external alternating electromagnetic field leads to a significant increase in the probability of quasiparticle tunneling through the barrier in the SIS junction [14]. This leads to the appearance of a so-called quasiparticle step on the IVC that is displaced by a voltage of hf/e from the gap (f is the frequency of the external signal); the current on it is used to estimate the fraction of power having passed through the circuit (see Fig. 2, dashed line).

A dc block represented as a slot antenna is located in the circuit between the generator on the FFO and the SIS detector. Such a structure allows their independent dc connection and, at the same time, provides transmission of a microwave signal. To detune the capacitance of the SIS junction, the circuit contains a radial stub, which introduces additional inductance. The circuit for matching of FFO, SIS detector, and dc break is implemented using step impedance transformers in the form of microstrip lines of a certain thickness. The geometric dimensions were chosen for each sample to provide the best signal transmission in the required range.

The technology for manufacturing of superconducting thin-film integrated multilayer structures studied in this work has been described by many authors [15–17].

2. DESCRIPTION OF MODELS

2.1. Semi-Analytical Model

In the simulation of the structures under study using the ABCD-matrices (transfer matrices) method, each element of the circuit is represented as a matrix [9, 10, 18]. Multiplication of the ABCD matrices of all elements in the appropriate order yields a transfer matrix of the entire structure. Expressions for the impedance of a slot antenna can be found, for example, in [19].

The results of [20, 21] show that the propagation constant and characteristic impedance of a microstrip line with superconducting electrodes differ from those of a perfect microstrip due to the penetration of the magnetic field into the electrodes. Accurate calculations taking into account fringe effects yield the expressions [20]:

$$Z_0 = \frac{\eta_0}{\sqrt{\epsilon_{\text{eff}}}}\sqrt{g_1^2 - \frac{jg_1g_2\left(Z^{\text{u}} + Z^{\text{l}}\right)}{k_0\eta_0}},$$
$$\gamma = \sqrt{-k_0^2\epsilon_{\text{eff}} + \frac{jg_2k_0\epsilon_{\text{eff}}\left(Z^{\text{u}} + Z^{\text{l}}\right)}{\eta_0 g_1}}, \quad (1)$$

where η_0 is the wave impedance of vacuum, k_0 is the wave vector of the wave in free space, ε_{eff} is the effective permittivity of the insulator layer corrected for field inhomogeneity in the microstrip line, g_1 takes into account effects of fringing field related to the finite thickness of the electrodes and the field outside the line, and g_2 takes into account penetration of the magnetic field into the electrodes. Surface impedances Z^{u} and Z^{l} of the upper and lower electrodes, respectively, were calculated using the expressions of the Mattis–Bardeen theory [22]. Weaker effects related to the finite free-path time [23, 24] turn out to be insignificant for films produced by magnetron sputtering due to small value of the mean free path [25].

The IVCs of the SIS detector in the presence of an external alternating signal can be calculated using the known autonomous IVC with the aid of expressions from [14]. The differential resistance near the operation point (at the quasiparticle step closest to the gap) at high frequencies can be considered approximately equal to R_n. At high frequencies, the capacitance of the SIS junction must also be taken into account. In addi-

tion, the presence of an SIS junction causes significant changes of the current flows in the electrodes of microstrip. To take this effect into account, we add an inductive term to the impedance of the SIS junction:

$$L_{\text{spread}} = 4\pi\left(\lambda_u \coth\left(\frac{d_u}{\lambda_u}\right) + \lambda_l \coth\left(\frac{d_l}{\lambda_l}\right) + \frac{H}{2}\right)\ln\left(\frac{R_{\text{ext}}}{R_{\text{SIS}}}\right), \quad (2)$$

where λ_u, λ_l and d_u, d_l are the penetration depths of the magnetic field and thickness of the upper and lower electrodes, respectively; H is the thickness of the insulator layer; R_{SIS} is the radius of the SIS junction; and R_{ext} is the characteristic distance at which the current lines are significantly bent. In all calculations, R_{ext} was chosen to be 3 μm.

A significant limitation of this model is the assumption that only longitudinal (quasi-TEM) modes are possible in the lines [21]. The use of multistep impedance transformers, needed for matching of the dc block, both with the generator and with the detector on the SIS junction leads to a significantly non-plane wavefront at the interface of two microstrip lines. However, in most systems, the length of such fragments is much less than the length of microstrips on which the wavefront is plane and, therefore, the experimental characteristics only slightly differ from the calculated ones.

2.2. Simulation in Ansys HFSS

In Ansys HFSS, microwave fields in a structure are calculated using the finite element method with an adaptive mesh: the structure is successively divided into tetrahedrons and each subsequent division is performed in areas with the greatest change in the field upon passage through the boundary of the tetrahedrons at the previous step. Solutions to the Maxwell equations are found as polynomials (by default, linear) using minimization of functional $\iint \varphi\Delta\varphi d^3r$ [26], where φ is the electrostatic potential and integration is performed over the entire volume.

Signal excitation and reception in 3D simulators are carried out using ports. In fact, a port represents a certain plane for which, first, eigenmodes are found and, then, the solution becomes the boundary condition for a 3D problem. In this work, it turned out to be most convenient to use lumped ports due to the fact that the port corresponding to the SIS detector must be located inside the simulated region, where installation of a wave port is impossible.

Simulation of structures in 3D simulators is somehow easier with respect to correct taking into account fringe effects and field distribution, as well as the mutual effect of elements. However, most commercial programs do not have a built-in module that would allow them to take into account the superconducting properties of materials.

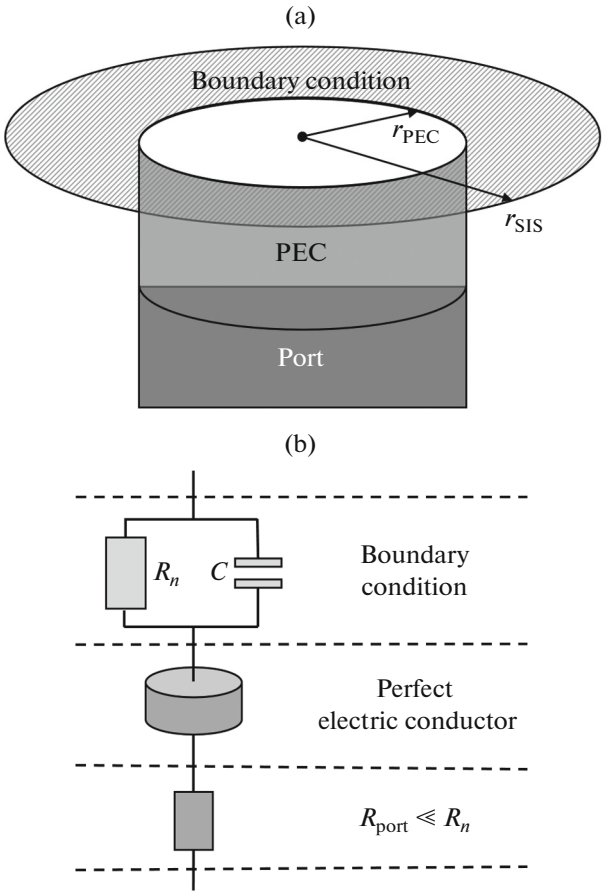

Fig. 3. (a) Scheme for connection of the SIS junction to a microstrip line for the Ansys HFSS simulation and (b) equivalent circuit.

To solve the problem, we propose setting of the boundary conditions on the surfaces of objects corresponding to the superconducting electrodes of the transmission line. The results of [28, 29] show that good agreement between the simulated and experimental results can be achieved with the correct setting of boundary conditions.

In all systems under study, the SIS junction is used to directly detect the signal. The SIS junction was installed as shown in Fig. 3 to take into account the change in current flow in the vicinity of the lumped SIS junction and to be able to set the port directly on it. Lumped port R_{port} (see Fig. 3a) is represented as a rectangle touching the lower electrode and a cylinder made of perfect electric conductor r_{PEC}. The height and radius r_{PEC} of the perfectly conducting cylinder do not affect the calculated results. The perfect conductor is surrounded by a ring, the outer radius of which is equal to the radius of the SIS junction in the sample and the inner radius is equal to the radius of the cylin-

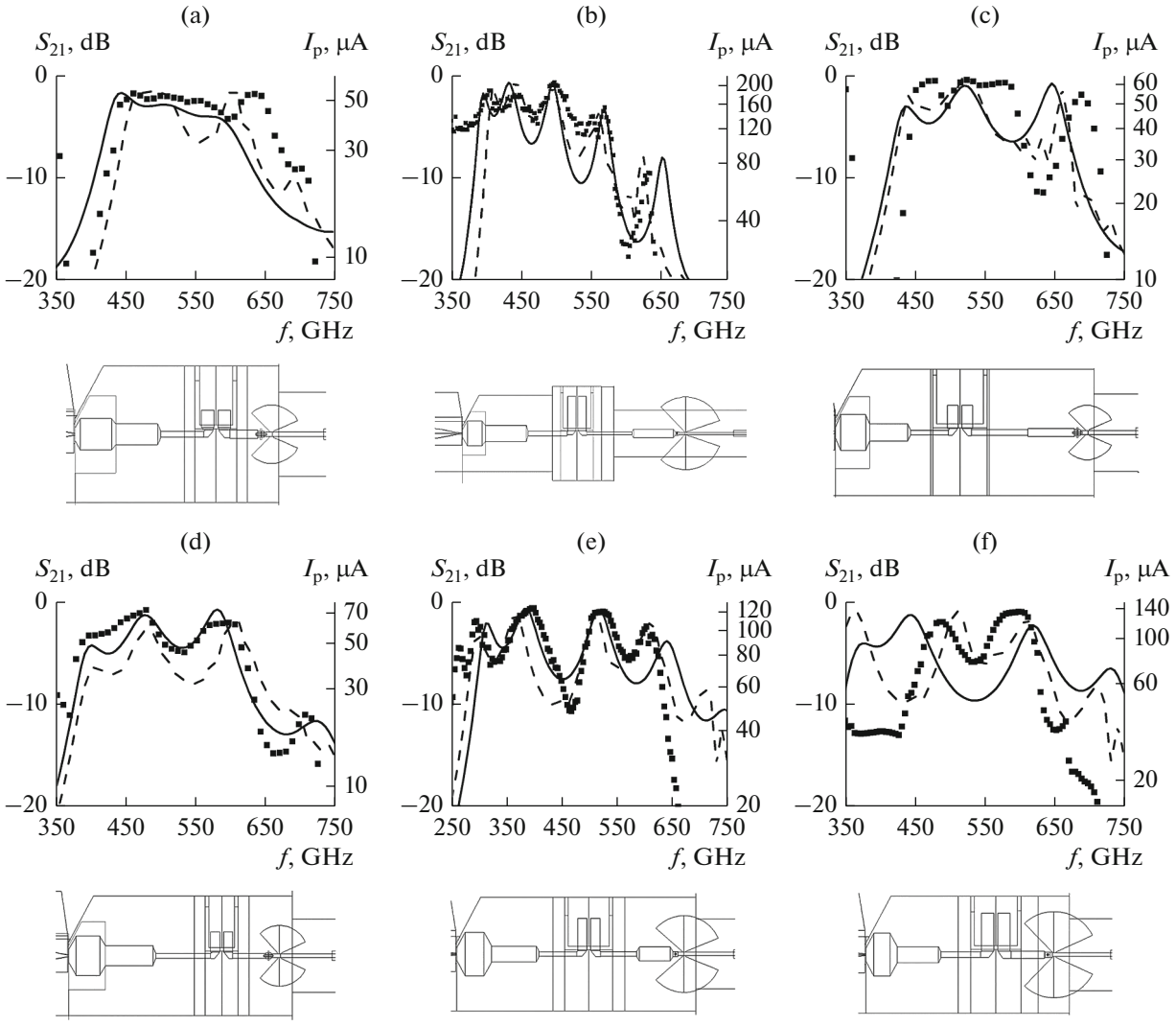

Fig. 4. Results of (solid line) semi-analytical calculation and (dashed line) Ansys HFSS calculation of the S_{21} parameter for simulated structures and (solid squares) experimental data I_p (the corresponding structure is shown below each plot): (a), (d), and (f) samples with a single-section impedance transformer between the SIS detector and the dc break (see item *4* in Fig. 1); (b), (c), and (d) samples with two-section transformer. The areas of the SIS detectors are (a) 0.67, (b) 2.55, (c) 0.87, (d) 0.69, (e) 1.05, and (f) 1.3 μm^2.

der. The boundary conditions on the ring correspond to impedance Z_{SIS} of the parallel-connected capacitance of the SIS junction and R_n (normal-state resistance). When recalculated per square of the surface, the boundary conditions correspond to the expression

$$Z_{\square} = Z_{SIS}\frac{2\pi}{\ln\left(r_{SIS}/r_{pc}\right)}. \quad (3)$$

Figure 3b shows an equivalent circuit. To make a transition from the power detected by the port to the total power arriving at the SIS junction, we must use the expression obtained using the Kirchhoff rule:

$$S_{21}^{SIS} = S_{21}^{port} + 10\log\left(1+\frac{\mathrm{Re}\left(Z_{SIS}\right)}{R_{port}}\right), \quad (4)$$

where R_{port} is the port resistance, which, in all simulations, was chosen to be 1 mΩ (much less than $\mathrm{Re}(Z_{SIS})$).

3. DISCUSSION

Figure 4 presents calculations performed using both models and experimental results. In total, we simulated more than 10 samples with different topologies and parameters of SIS junctions. The areas of SIS junctions in the samples under study range from 0.5 to 2.5 μm^2, and the tunneling current densities range from 5 to 25 kA/cm^2. Each sample is designed to provide the best matching in the required range. For most structures, the positions of specific features on the S_{21} curves calculated using both models coincide in fre-

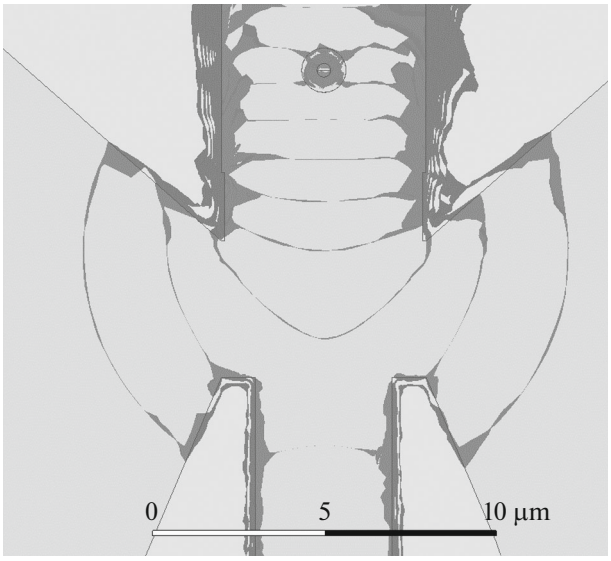

Fig. 5. Distribution of the electric field amplitude at a frequency of 500 GHz near the transition from the SIS detector to the radial stub with an outer radius of 48 μm calculated using Ansys HFSS; the constant-phase surfaces are strongly curved.

quency with the measured response of the SIS junction.

Note that a generator based on a distributed Josephson junction is a complicated dynamic system, with strong nonlinearity. Thus, the signal at the fundamental frequency is supplemented with waves with multiple frequencies. This circumstance accounts for the difference between calculated and experimental results at frequencies of less than 350 GHz. It is also difficult to estimate the power generated by the FFO, and we can only talk about qualitative agreement between calculated and experimental results.

As was mentioned in Section 2, the semi-analytical calculation assumes propagation of a quasi-TEM wave in the lines, in other words, the constant-phase surfaces have a plane front perpendicular to the edges of the microstrip lines. Therefore, the results of semi-analytical calculation for the sample in Fig. 4e do not correspond to experimental and Ansys HFSS results. Figure 5 shows the curvature of the wavefront between the SIS junction and the radial stub.

CONCLUSIONS

We simulated superconducting integrated structures using two methods, the results of which are in qualitative agreement both with each other and with the experimental data. The implemented programs already made it possible to design samples that cover an entire interval of 400–650 GHz at a level of no less than -3 ± 1 dB. A number of samples were fabricated and successfully tested, and several new samples are being prepared for production. The methods outlined in this work are applicable for a wide class of structures and are already used in the design of superconducting receivers and generators.

ACKNOWLEDGMENTS

The authors are grateful for the access to the unique scientific unit “Cryointegral” (USU no. 352529), which was used for preparation of samples and measurements.

FUNDING

The development and study of the structures was supported by the Russian Science Foundation, project no. 23-79-00019, https://rscf.ru/project/23-79-00019/. Numerical calculations were carried out within the framework of the state task at Kotelnikov IREE of RAS. The operation of USU “Cryointegral” was supported by the Ministry of Science and Higher Education of the Russian Federation, agreement RF-2296.61321X0041.

CONFLICT OF INTERESTS

The authors declare that they have no conflicts of interest.

REFERENCES

1. T. Kojima, M. Kroug, M. Takeda, et al., Appl. Phys. Express **2**, 102201 (2009). https://doi.org/10.1143/APEX.2.102201
2. G. De Lange, M. Birk, D. Boersma, et al., Superconductor Sci. Technol. **23**, 045016 (2010). https://doi.org/10.1088/0953-2048/23/4/045016
3. B. Billade, A. Pavolotsky, and V. Belitsky, IEEE Trans. on Terahertz Sci. & Technol. **3**, 416 (2013). https://doi.org/10.1109/TTHZ.2013.2255734
4. V. V. Schmidt, *Introduction to the Physics of Superconductors* (MTsNMO, Moscow, 2000).
5. K. A. Baksheeva, R. V. Ozhegov, G. N. Goltsman, et al., IEEE Trans. on Terahertz Sci. & Technol. **11** (4), 381 (2021). https://doi.org/10.1109/TTHZ.2021.3066099
6. N. V. Kinev, K. I. Rudakov, L. V. Filippenko, V. P. Koshelets, et al., Phys. Solid State **63**, 1414 (2021). https://doi.org/10.1134/S1063783421090171
7. A. M. Barychev, “Superconductor-Insulator-Superconductor THz Mixer Integrated with a Superconducting Flux-Flow Oscillator,” PhD Thesis, (Delft Univ. Technol., Delft, 2005).
8. Ya. O. Vodzyanovskii, A. V. Khudchenko, and V. P. Koshelets, FTT. **64**, 1385 (2022).
9. V. Fusko, *Microwave Circuits* (Prentice-Hall Collection Inlibrary, Englewood Cliffs, 1987; Radio i Svyaz’, Moscow, 1990).
10. D. A. Frickey, IEEE Trans. Microwave Theory Tech. (T-MTT) **42** (2), 205 (1994). https://doi.org/10.1109/22.275248
11. M. S. Shevchenko, L. V. Filippenko, O. S. Kiselev, and V. P. Koshelets, FTT **64**, 1223 (2022).

12. V. P. Koshelets, S. V. Shitov, L. V. Filippenko, et al., Superconducting Sci. Technol. **17** (127) (2004). https://doi.org/10.1088/0953-2048/17/5/007
13. V. P. Koshelets and S. V. Shitov, Superconductor Sci. Technol. **13** (5), 53 (2000). https://doi.org/10.1088/0953-2048/13/5/201
14. J. R. Tucker and M. J. Feldman, Rev. Mod. Phys. **57** (4), 1055 (1985). https://doi.org/10.1103/RevModPhys.57.1055
15. L. V. Filippenko, S. V. Shitov, P. N. Dmitriev, et al., IEEE Trans. Appl. Supercond. **11** (1), 816 (2001). https://doi.org/10.1109/77.919469
16. M. Yu. Fominsky, L. V. Filippenko, A. M. Chekushkin, et al., Electronic. **10** (23), 2944 (2021). https://doi.org/10.3390/electronics10232944
17. S. K. Tolpygo, V. Bolkhovky, T. J. Weir, et al., IEEE Trans. Appl. Supercond. **25** (3), 1 (2014). https://doi.org/10.1109/TASC.2014.2369213
18. A. A. Atepalikhin, F. V. Khan, L. V. Filippenko, and V. P. Koshelets, FTT. **64**, 1378 (2022).
19. S. V. Shitov, "Integral devices at superconducting tunnel junctions for millimeter and submillimeter wave receivers," Doctoral Disssertation (Phys. Math) (IRE im. V. A. Kotel'nikova RAN, Moscow, 2003).
20. G. Yassin and S. Withington, J. Phys. D: Appl. Phys. **28** (9), 1983 (1995). https://doi.org/10.1088/0022-3727/28/9/028
21. J. C. Swihart, J. Appl. Phys. **32** (3), 461 (1961). https://doi.org/10.1063/1.1736025
22. D. C. Mattis and J. Bardeen, Phys. Rev. **111** (2), 412 (1958). https://doi.org/10.1103/PhysRev.111.412
23. W. Zimmermann, E. H. Brandt, M. Bauer, et al., Physica C: Superconductivity **183** (1–3), 99 (1991). https://doi.org/10.1016/0921-4534(91)90771-P
24. R. Pöpel, J. Appl. Phys. **66** (12), 5950 (1989). https://doi.org/10.1063/1.343622
25. S. B. Nam, Phys. Rev. **156** (2), 470 (1967). https://doi.org/10.1103/PhysRev.156.470
26. S. E. Bankov, A. A. Kurushin, and V. D. Razevig, *Analysis and Optimization of Three-dimensional Microwave Structures with the Help of HFSS. Manual* (Solon, Moscow, 2005) [in Russian].
27. A. R. Kerr and S. K. Pan, Int. J. Infrared & Millimeter Waves **11** (10), 1169 (1990). https://doi.org/10.1007/BF01014738
28. V. Belitsky, C. Risacher, M. Pantaleev, and V. Vassilev, Int. J. Infrared and Millimeter Waves **27** (1), 809 (2006). https://doi.org/10.1007/s10762-006-9116-5

Translated by A. Chikishev